Supplementary Online Content

Holland D, Chang L, Ernst TM, Curran M, Buchthal SD, Alicata D, Skranes J, Johansen H, Hernandez A, Yamakawa R, Kuperman JM, Dale AM. Structural growth trajectories and rates of change in the first 3 months of infant brain development. *JAMA Neurol*. Published online August 11, 2014. doi:10.1001/jamaneurol.2014.1638.

eIntroduction.

eMethods.

eResults.

eTable 1. Comparison of automatic and manual segmentation.

eTable 2. Whole-brain growth trajectories: model results

eTable 3. Whole-brain growth trajectories: model results

eFigure 1. Comparison of manual and automatic segmentation

eFigure 2. Whole-brain growth trajectories, including controlling for head circumference at birth

eFigure 3. Volume-for-age percentile plots, and residualized volume-for-age percentile plots

eFigure 4. Growth trajectories and rates of change for caudate, cerebellum, putamen, and lateral ventricles.

eFigure 5. Growth trajectories and rates of change for amygdala, hippocampus, thalamus, and brain stem.

eFigure 6. Volume-by age percentile plots for caudate, cerebellum, putamen, and lateral ventricles.

eFigure 7. Spaghetti plot of volume difference between left and right lateral ventricles

eFigure 8. Spaghetti plots of volume difference between left and right ROIs, for amygdala, hippocampus, caudate, thalamus, putamen, and cerebellum.

eReferences.

This supplementary material has been provided by the authors to give readers additional information about their work.

eIntroduction

Structural development and abnormalities
Abnormalities in gray and white matter volumes have been documented in many neurodevelopmental conditions, including those with known or putative genetic bases, such as Down syndrome[1,2], William syndrome[3], fragile X syndrome[4,5], autism[6], and schizophrenia[7], as well as those associated with pre- or perinatal injury to the brain, such as perinatal stroke, hypoxic-ischemic encephalopathy, hypoglycemia[8], extreme prematurity, and *in utero* exposure to teratogenic agents. Better understanding of when and how structural correlates of these disorders arise in the postnatal period may help illuminate their etiology and assist in therapeutic development, with the possibility that early intervention during a period of high neuroplasticity would mitigate the severity of the disorders in later years. The ability to perform quantitative longitudinal structural analysis additionally allows for assessing developmental trajectories of newborns who suffer from high-risk conditions, who may not show cognitive deficits until their school years[9,10], as well as for assessing response to therapeutic intervention[11].

eMethods

Participant Enrolment and Study Criteria
A total of 572 parents were screened initially by telephone or at the local hospital and clinics; 180 parents or legal guardians signed a written informed consent, approved by the Institutional Review Board at the University of Hawaii. After detailed interviews with the parents or legal guardians regarding the mother's medical and drug use histories, 87 healthy neonates (39 male and 48 female) fulfilling study criteria were enrolled for the current MR study. At first scan, postmenstrual age[12] (±standard error) was 40.7±0.2 weeks (range 36 to 49; postmenstrual age at birth was 38.6±0.2 weeks, range 28.3 to 41.3). 57 neonates returned for follow-up scans approximately one-month later and 49 neonates returned again for their two-month follow-up scans. All infants were evaluated thoroughly with birth record reviews and a clinical neurological examination to ensure they fulfilled the following inclusion criteria: (1) newborn approximately 1 week old, male or female of any ethnicity; (2) parental or legal guardian consent for the infant to participate in the study. Exclusion criteria for the infant include: (1) any known neurological disorders or abnormalities; (2) newborn illness requiring >1 week intensive care; (3) intracranial hemorrhage; (4) hypoxic ischemic encephalopathy; (5) overt perinatal TORCH (Toxoplasmosis, Other, Rubella, Cytomegalovirus or Herpes Simplex) infection at birth or a major neurological disorder since birth; (6) any chromosomal anomaly; (7) other contraindications for MR studies; (8) if the mother was unable to provide consent due to age ≤17 years at the time of childbirth or unable to fully understand English; (9) if the mother tested positive for HIV infection; (10) if the mother had smoked tobacco cigarettes or used excess alcohol (>3 drinks/month) during the pregnancy.

Subject Characteristics

Table 1 shows the clinical characteristics of the 87 infants. The male and female infants were born at similar postmenstrual age, had similar birth weight, birth length, and head circumference. At the time of their baseline scans the weight, length, and head circumference remained similar between the boys and the girls. The majority of the neonates were born by vaginal delivery. None of these infants had birth complications as shown by the normal APGAR scores at 1 minute and 5 minutes. At delivery, their mothers were 29.3±0.7 years of age, with no difference between those that gave birth to the boys or the girls. The neonates also had similar nutritional status as indicated by the similar weight gain by their mothers during the pregnancies; averaged weight gain was 14.4±0.8 kg. These infants were primarily mixed race (54%), and the remainder included Caucasian (non-Hispanic, 8%), Native Hawaiian/Pacific Islander (22%), Asian (13%) and Black (1%). Only four male participants were from two pairs of twins, but all other participants were singletons.

Image Acquisition

T_1 and T_2 weighted MRI scans were acquired with three-dimensional pulse sequences on a Siemens TrioTim 3.0 T scanner (Siemens Medical Systems, Erlangen, Germany) while the infant slept without sedation. Prior to scanning, the infants were fed by the mothers and allowed to fall asleep naturally. Ear protection included infant earplugs and earphones. Infants were wrapped in a vacuum immobilization mat (Noras MRI Products, Hoechberg, Germany) to minimize motion. A 12-channel head array from Siemens/MRI Devices was used. The MRI began with a 3 orthogonal directions T_1-weighted localizer (echo time/relaxation time or TE/TR = 5/20 ms, 10-mm slice thickness, 2-mm gap, 256-mm field of view). For the T_1-weighted scans, an MPRAGE sequence was acquired with the following parameters: TR = 3200 ms, TE = 4.15 ms, TI = 1400 ms, flip angle = 9°. The matrix size was 256×176, with 160 slices of 1 mm thickness, leading to a spatial resolution of $1\times1\times1$ mm^3. For the T_2-weighted scans, a Turbo Spin-Echo SPACE sequence was acquired with the following parameters: TR = 3200 ms, TE = 386 ms, flip angle =120°, matrix size 256×204, with 120 slices of 1 mm thickness, leading to a spatial resolution $1\times1\times1$ mm^3.

Severe image degradation due to excessive subject motion during scan acquisition required that 24 infants had one repeat scan and three infants had two repeat scans on different days (the remaining 60 infants did not require repeat scans), to yield a total of 233 final MRI scan sessions. After ensuring visually that the T_1 or the T_2 scan was of sufficiently high quality that the whole brain was reasonably well-defined, a total of 211 subject-timepoints, or scan-visits, from the full set of 87 subjects were included in the analysis (9.4% failure rate; Table 1). For 135 subject-timepoints, both T_1 and T_2 scans were useable, allowing bimodal segmentations to be produced as described below; for 69 subject-timepoints only the T_1 was useable, and for 7 subject-timepoints only the T_2 scan was useable.

Tissue Segmentation

All T_1- and T_2-weighted images were first corrected for geometric distortion due to non-uniformity in the scanner gradient field[13] and re-sampled using cubic interpolation to 256^3 voxels of size $0.6\times0.6\times0.6$ mm^3. Single time-points from 24 subjects with high quality T_1 and T_2 scans in which tissue regions could be well-defined were then chosen for manual segmentation of twelve sub-regions, eight of which were bilateral: left and right cerebellum, thalamus, caudate, putamen, pallidum, hippocampus, amygdala, and lateral ventricles; brain stem, 3rd ventricle, 4th ventricle, and a region covering the brain parenchyma and ventricles but excluding cerebellum and brain stem. "Whole brain" as used here excludes ventricles but includes both cerebellum and brain stem. The mean postnatal age for these 24 subjects when scanned was 55.4±5.7 days (range 6.0 to 122.0; the mean postmenstrual age at scan time was 46.4±0.9 weeks, range 36 to 52).

Aligned T_1- and T_2-weighted atlas images were built separately in an iterative fashion, first by selecting a manually segmented 69-day-old as a target (postmenstrual age at scan 58.9 weeks), 12-parameter affine registering the other manually segmented images to it, and averaging. A more sharply defined average image was then generated by nonlinearly registering the affine registered images to the target and again averaging, producing a new target; nonlinear registration and correction of intensity nonuniformity was performed using a modified version of Quarc[14,15] (*qu*antitative *a*natomical *r*egional *c*hange), a recently developed method from our laboratory. Subsequently, a total of 96 images were repeatedly aligned and averaged until no discernable improvement could be detected in the target (8 iterations). Coronal, axial, and sagittal slices of the T_1 and T_2 atlas images are shown in Figure 1(A).

T_2 images were rigid-body (6-parameter) registered to the corresponding T_1 images by maximization of mutual information[16,17]. To do this, the subject's T_1 scan first had to be fully (12-parameter) affine mapped to the atlas T_1. Given the wide range in brain sizes and variation in shapes, this required an iterative scheme to estimate the uniform scaling (increase or decrease) of the subject's image to make it roughly the size of the atlas while simultaneously rigid-body aligning to the atlas. Finally, a full affine registration to the atlas was performed. The inverse mapping was then applied to the atlas brain mask to produce a brain mask in the subject's native space. The subject's brain mask was then used to rigid-body register the subject's T_2 to T_1 by maximization of mutual information.

Automatic segmentation can be performed by maximizing at each location $\mathbf{r} = (r_x,r_y,r_z)$ the probability $p(S(\mathbf{r})|\mathbf{I}(\mathbf{r}))$ of a given segmentation (tissue label) $S(\mathbf{r})$ given the multispectral intensities $\mathbf{I}(\mathbf{r})$ at that location. This quantity is proportional to the product $p(\mathbf{I}(\mathbf{r})|S(\mathbf{r}))\times p(S(\mathbf{r}))$, where $p(\mathbf{I}(\mathbf{r})|S(\mathbf{r}))$ is the likelihood of T_1 and T_2 image intensities $\mathbf{I}(\mathbf{r}) = (I_1(\mathbf{r}),I_2(\mathbf{r}))$ occurring, given the segmentation $S(\mathbf{r})$, and $p(S(\mathbf{r}))$ is the prior probability of segmentation $S(\mathbf{r})$. The prior probabilities and likelihood function are built from mapping the manually segmented images and their segmentations to the atlas. All mappings to atlas were performed using Quarc. At atlas location $\mathbf{r}$, the prior for any given tissue type is simply the fraction of manually segmented images which, upon mapping to the atlas, have that tissue type at $\mathbf{r}$. For any given multispectral image, the priors in native image space can be found by inverting the mapping of the component images to atlas space and then applying the inverse mapping to the atlas space priors. The likelihood function (for multispectral intensities, given a particular segmentation) can be built in native image space by constructing a histogram, over the full range of intensities, for the

frequency of occurrence of voxels of given multispectral intensities (I_1,I_2) within the spatially-defined prior. Automatic segmentation of each image was performed independently of the automatic segmentation of all other images.

Evaluation of Automatic Tissue Segmentation

To evaluate the validity of the automatic segmentation procedure, for the 24 subject time-points that were manually segmented we compared it with the manual segmentation using absolute structure volumes along with two additional metrics: percent overlap and percent difference (normalizing by the average of the volumes from automatic and manual segmentation)[18]. Given two segmentations S_A and S_M for a tissue structure, and letting V(.) denote the corresponding volume, the percent volume overlap is given by

$$O(S_A, S_M) = 100 \times V(S_A \cap S_M) / (V(S_A) + V(S_M)) / 2, \quad \text{(e1)}$$

where $S_A \cap S_M$ denotes voxels labeled the same by both methods, and the percent volume difference is given by

$$D(S_A, S_M) = 100 \times |V(S_A) - V(S_M)| / (V(S_A) + V(S_M)) / 2. \quad \text{(e2)}$$

O(.) is also known as the Sørensen index or Dice coefficient. Note that O is sensitive to relative spatial shifts in the tissue labels, while D is insensitive. Higher values of O and lower values of D indicate greater consistency and statistical power to detect volumetric change.

Estimation of Adult Brain Volume

Whole-brain volume in humans is known to peak in the teenage years and slowly decrease thereafter[19-22]. For the purpose of providing an illustrative comparison of infant brain volumes with a well-defined measure for adult brain volume (including cerebellum and brain stem, excluding ventricles, and averaging over both sexes), an estimate of the latter was calculated from 182 healthy elderly enrolled in the Alzheimer's Disease Neuroimaging Initiative (ADNI, www.adni-info.org) using standard procedures[13], for whom the mean age was 76.1±0.4 years (range 59.8 to 90.2).

Controlling for head circumference or body length at birth

Along with gestation age at birth and sex, other factors may affect brain size at birth, and are thus likely to have an effect on longitudinal brain sizes (for example, people genetically predisposed to be taller will tend to have larger heads). Although direct measures of brain volume at birth were unavailable in this study, it is of interest nevertheless to control for brain size at birth while simultaneously controlling for gestation age and sex, so as to finesse the effects of these latter two on structural brain development. Two proxies for brain size at birth are brain circumference and body length. These were used, one at a time, as additional covariates in a modified version of the Equation in the main article (hereafter Eqn. (1)). Specifically, we added a term c_0C_i for subject i, where C_i is the mean-centered head circumference or body length at birth for that subject, and c_0 is a cohort coefficient to be determined:

$$Y_{ij} = f(t_{ij}) + c_0C_i + g_0G_i + s_0S_i + g_tG_it_{ij} + s_tS_it_{ij} + \varepsilon_{ij}. \quad \text{(e3)}$$

To facilitate an appropriate "head-to-head" comparison of the effects of thus controlling or not controlling for brain size or body length at birth, analyses on whole brain were restricted to the subset of subjects who had data available for both brain circumference and body length at birth: 63 babies (28 males, 6 with baseline only; 35 females, 6 with baseline only), with 156 scan-visits (87 from females). Compared with the full data set modeled using Eqn. (1), a slight difference in mean trajectories might occur due to the fact that a subset of the subjects was used. The inclusion of the extra term (c_0C_i), however, is expected to reduce the variance in the male and female estimated trajectories.

Volume-for-age percentile plots

Volume-for-age percentile plots were recalculated as described in the main paper, but where the mean trajectories for boys and girls were estimated based on Eqn. (e3) and restricted to the 63 babies with measurements for both head circumference and body length at birth. Volume-for-age percentile plots were additionally calculated based on the residualized volumes obtained by subtracting from each subject's actual volume Y_{ij} at each time point j the amount $R_{ij} = (c_0C_i + g_0G_i + g_tG_it_{ij})$:

$$Z_{ij} = Y_{ij} - R_{ij}. \quad \text{(e4)}$$

Note that R_{ij} could instead be composed only of any one or any pair of the three terms given above; the more terms included the less variance or spread there should be in the resulting residualized volume-for-age percentile plots. The difference between Z_{ij} (for whole-brain volume) for each subject-timepoint and the respective male or female best-fit growth trajectory from Eqn. (e3) was calculated, and the squares of these were fit as a smooth function of age using GAMM. For males and females, the square root of the fit provided the estimate for the standard deviation of the spread in residualized volume around the respective mean as a function of age. Residualized volumes for various percentiles were then estimated from the inverse of the corresponding normal cumulative distribution function. To use these plots to assess the percentile of any new infant aged d (in days), whose brain volume is Y (in mm^3), gestation age at birth is G (in days), and head circumference (or body length) at birth is C (in mm), one simply computes $R = (c_0 \times C + g_0 \times G + g_t \times G \times d)$ using the coefficients c_0, g_0, and g_t given below in Tables S2 and S3. The baby's residualized brain volume is then given by $Z = Y - R$, and the baby's percentile can simply be read off from the point (d, Z) in the appropriate residualized-volumes-for-age percentile figure – eFigure 3(B) or eFigure 3(D).

eResults

Comparison of Automatic and Manual Segmentation

Results for absolute structure volumes (with standard errors of the means) are shown in eFigure 1(A) (numerical values are in eTable 1). The automatic procedure tends to comparatively underestimate the ventricular volumes, but the outcomes are not significantly different for most

other structures. The manual and automatic segmentation volumes are not significantly different for the whole brain and for the cerebellum. For example, the estimated whole-brain volume from manual segmentation is 474,591 mm^3, 95% CI = [463,251; 485,931], while from automatic segmentation the volume is 481,275 mm^3, CI = [469,535; 493,015] (p = 0.7).

Results for percentage overlap and difference, as defined by Eqns. (e1) and (e2), are shown in eFigures 1(B) and 1(C). Most regions show a volume overlap above 80% and difference below 25%; however, some of the smaller regions have poorer accuracies. Greatest accuracy is found for the whole brain, showing highest overlap (O = 95.3%, standard error of the mean = 0.1%) and lowest difference (D = 1.8%, standard error SE = 0.4%)

Examples of results of automatic segmentation (coronal, axial, and sagittal slices), for two male subjects who were not manually segmented, are shown in Figure 1(B).

Controlling for head circumference or body length at birth

Restricting analysis to the 63 subjects with measures for both head circumference and body length at birth, growth trajectories were recalculated using Eqn. (1). The results shown in eFigure 2(A), with numerical values in eTables 2 and 3 (1st row), are largely consistent with those based on the full data set (Figure 2(A) in the main paper). As expected, almost identical mean trajectories for males and females were found when head circumference or body length at birth was additionally covaried for using Eqn. (e3), while the standard error was slightly reduced. The resulting trajectories are plotted in eFigure 2(B), with numerical values in eTables 2 and 3 (2nd and 3rd rows). However, male and female brain volumes at birth were found to be significantly different: males larger than females by approximately 5% of female brain volume. (Using Eqn. (1), the difference between male and female brain volumes did not reach statistical significance until one week after birth.) Related to this, the sex effect (s_0 coefficient) was significant. At 90 days, the whole-brain volume difference between the sexes had increased to 6.7% of female brain volume. Both head circumference and body length at birth were significantly associated with brain size at birth, though as might be expected the stronger association was with head circumference: for each additional millimeter in circumference, brain volume was larger by $c_0 \times 1\text{mm} = 11.8\ cm^3$ (SE = 2.3 cm^3, $p = 10^{-6}$). Duration of gestation is closely correlated with head circumference and body length at birth, and is significantly associated with brain volume. Nevertheless, when covarying for head circumference or body length at birth, its effect on brain volume remained significant, though the size of the effect approximately halved. For example, when not covarying for length or circumference at birth, for each additional day above average that gestation lasted brain size was larger by $g_0 \times 1\text{day} = 1.99\ cm^3$ (SE = 0.332 cm^3, $p = 2 \times 10^{-8}$); in contrast, when covarying for head circumference at birth, for each day above average that gestation lasted brain size was larger by $g_0 \times 1\text{day} = 1.02\ cm^3$ (SE = 0.356 cm^3, p = 0.0048).

Volume-for-age percentile plots

Volume-for-age percentile plots were recalculated based on deviations from the mean trajectories estimated for the 63 subjects who had measures for both head circumference and body length at birth; the results are shown in eFigure 3(A) and 3(C). These are similar to the plots based on the full data set of 87 subjects (Figure 2(C) and 2(D), in the main paper). Since

additionally covarying for head circumference or body length at birth does not noticeably alter the mean trajectories, almost identical plots results when thus covarying. However, including these covariates, along with gestation age at birth, affords the possibility of assessing an individual on residualized volume-for-age percentile plots with substantially narrower spread – assuming values for these quantities at birth are known for the individual (so that residualized volume for his or her whole brain – or other region of interest – can be calculated). Residualized volume-for-age percentile plots based on the subset of 63 subjects are shown in eFigure 3(B) and 3(D). For example, on the residualized plots, the spread between the 95^{th} and 5^{th} percentiles at birth is only 61% of the corresponding spread on the standard (nonresidualized) plots. Deviation from the 50^{th} percentile on the residualized plots might be indicative of abnormal development insofar as the individual's values for the covaried variables themselves do not account for or mask pathology.

eTable 1. Comparison of Automatic and Manual Segmentation for 24 subjects

Measure	Manual Vol. (mm^3)	Manual 95% CI	Automatic Vol. (mm^3)	Automatic 95% CI	p-val
L Cerebellum	17502	[16865 18140]	18706	[17797 19615]	0.3
R Cerebellum	17349	[16705 17993]	18580	[17671 19488]	0.3
L Thalamus	2662	[2604 2719]	2694	[2620 2768]	0.7
R Thalamus	2689	[2627 2752]	2731	[2619 2842]	0.7
L Caudate	1683	[1636 1730]	1777	[1707 1847]	0.3
R Caudate	1625	[1582 1668]	1726	[1655 1796]	0.2
L Putamen	1622	[1579 1665]	1492	[1445 1538]	**0.04**
R Putamen	1715	[1672 1758]	1588	[1530 1646]	0.09
L Hippocampus	317	[305 328]	293	[277 310]	0.2
R Hippocampus	330	[319 341]	308	[285 330]	0.4
L Pallidum	142	[138 145]	118	[108 128]	**0.03**
R Pallidum	159	[155 164]	114	[105 124]	**0.0002**
L Amygdala	150	[144 156]	130	[119 141]	0.1
R Amygdala	126	[121 130]	121	[114 129]	0.6
Whole Brain	474591	[463251 485931]	481275	[469535 493015]	0.7
Brain-Stem	5346	[5195 5496]	5412	[5219 5605]	0.8
L Lat Ventricle	4273	[4082 4464]	3543	[3272 3813]	**0.03**
R Lat Ventricle	3736	[3584 3888]	2982	[2780 3183]	**0.005**
4th-Ventricle	653	[620 686]	469	[428 510]	**0.001**

Absolute structure volumes (with standard errors of the means) are shown in eFigure 1(A). Bold and underlined values are significant at the $\alpha = 0.05$ level.

eTable 2. Whole-brain growth trajectories: model results (continued on eTable 3)

Body measure at birth used as covariate	†Intercept (size at birth) [mm^3]					†Body Measure at Birth [c_0: mm^2]			†Gestation age [g_0: mm^3/day]		
	Male	SE	Female	SE	P	c_0	SE	P	g_0	SE	P
None$	353280	6844	337274	6119	0.083	–	–	–	**1990**	332	2×10^{-8}
Head Circum#	353389	5944	336755	5317	**0.039**	**11824**	2333	1×10^{-6}	**1020**	356	0.0048
Body Length#	354048	6262	336202	5602	**0.035**	**7207**	1816	0.00011	**1082**	386	0.0057

†Notation: c_0 and g_0 are model coefficients in Eqn. (e3), SE is standard error, and P is p-value. All results in this table are from the subset of 63 subjects who had values for head circumference and body length at birth. $Eqn. (1). #Eqn. (e3). Bold and underlined values are significant at the false-positive probability level of 5% (or $\alpha = 0.05$ level).

eTable 3. Whole-brain growth trajectories: model results (continued from eTable 2)

Body measure at birth used as covariate	Sex [s_0: mm^3]			†Gestation×Age [g_t: mm^3/day^2]			†Sex×Age [s_t: mm^3/day]		
	s_0	SE	P	g_t	SE	P	s_t	SE	P
None	-16006	8848	0.073	-6.7	3.5	0.054	**-223**	76	0.0040
Head Circum	**-16634**	7590	0.030	**-7.6**	3.4	0.027	**-226**	76	0.0035
Body Length	**-17846**	8046	0.028	-6.7	3.4	0.054	**-212**	76	0.0062

†Notation: s_0, g_t, and s_t are model coefficients in Eqn. (e3). See also eTable 2 for key.

eFigure 1

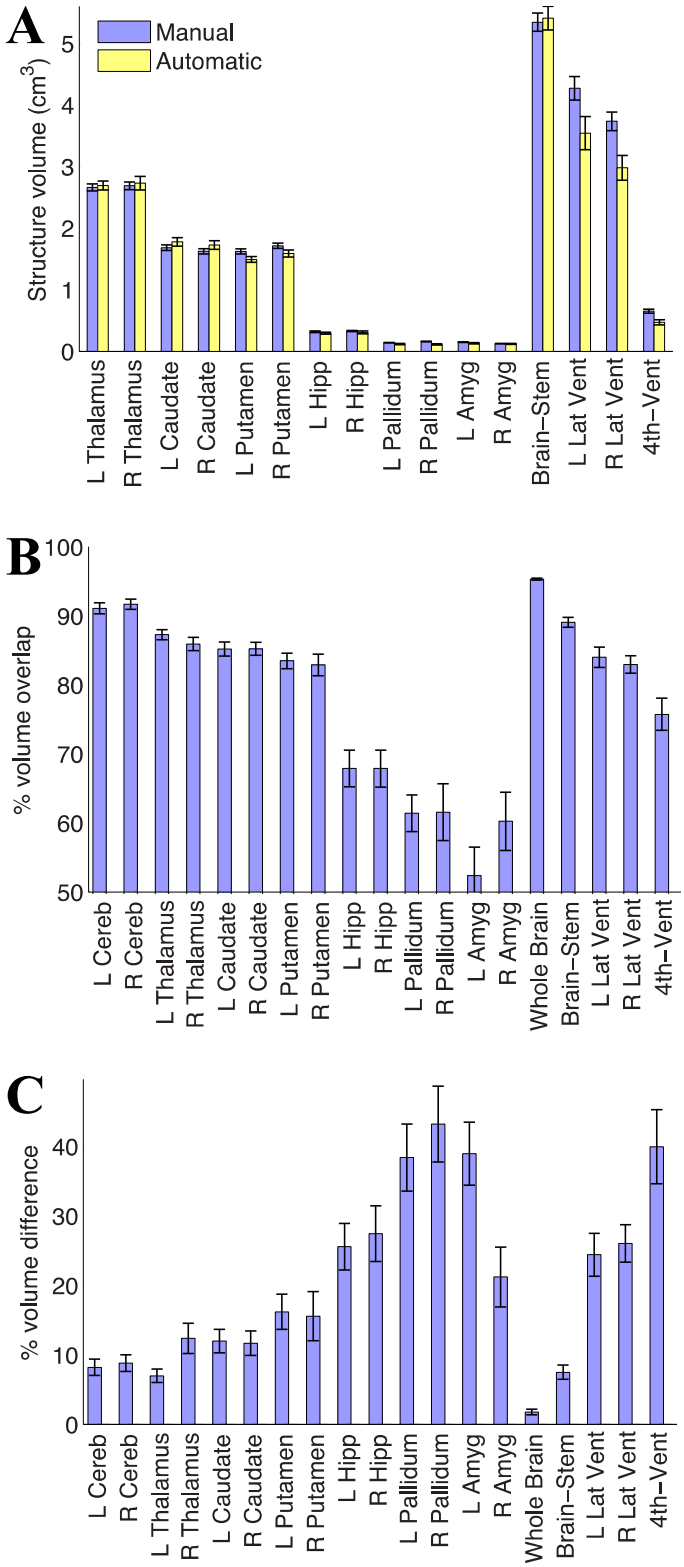

(A) Comparison of structure volumes computed from manual and automatic labeling, for the 24 subject time-points that were manually segmented. The error bars are standard errors of the

means. Reliability of manual with automated segmentations: (B) percentage volume overlap from Eqn. (1), and (C) percentage volume difference from Eqn. (2). See eTable 1.

eFigure 2

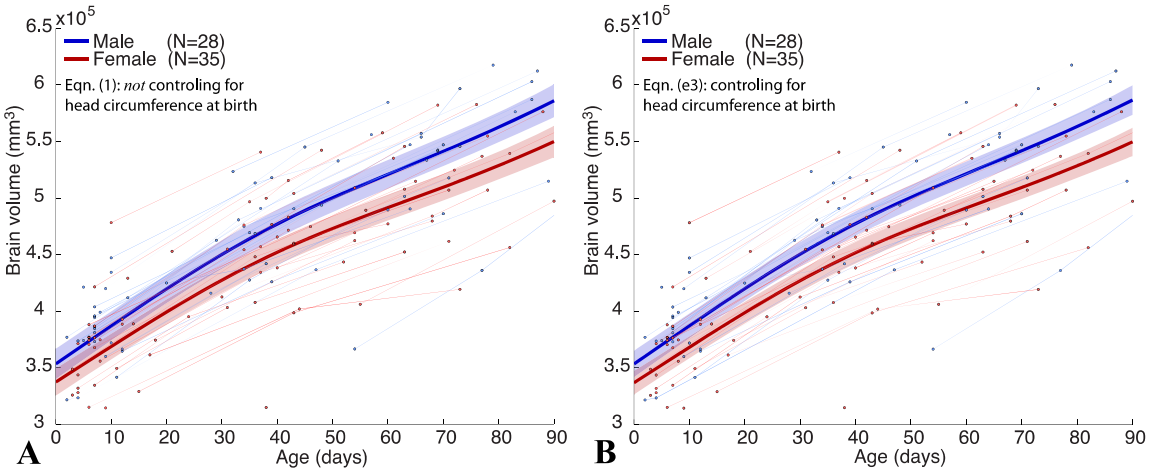

Spaghetti plot showing whole-brain volume during the first three months of postnatal life, along with GAMM fits to the data (dark lines), and 95% confidence intervals (shaded regions) for analyses based on the 63 subjects who had measures for head circumference and body length at birth. (A) GAMM fits modeled using Eqn. (1), i.e., not covarying for body size at birth. (B) GAMM fits modeled using Eqn. (e3), covarying for head circumference at birth. (Almost identical GAMM fits result when instead covarying for body length at birth.)

eFigure 3

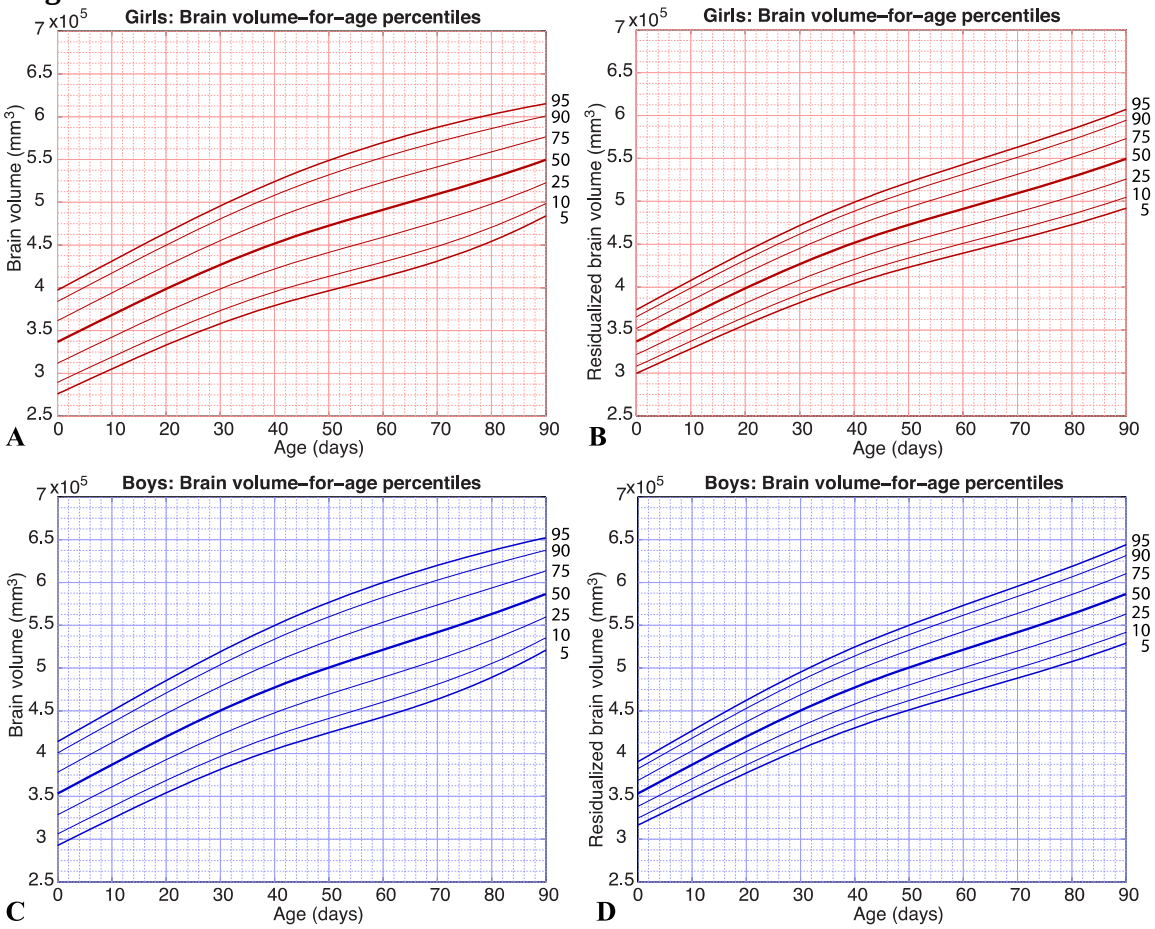

Volume-for-age percentile plots from analyses based on the 63 subjects who had measures for head circumference and body length at birth. (A) and (C) are for girls and boys, respectively, based on deviations from the mean trajectories calculated using Eqn. (e3), covarying for head circumference at birth; due to similarity in mean growth trajectories, almost identical plots result when not thus covarying. (B) and (D) are the corresponding plots residualizing brain volume with respect to the covariates gestation age at birth and head circumference at birth – see Eqn (e4).

eFigure 4

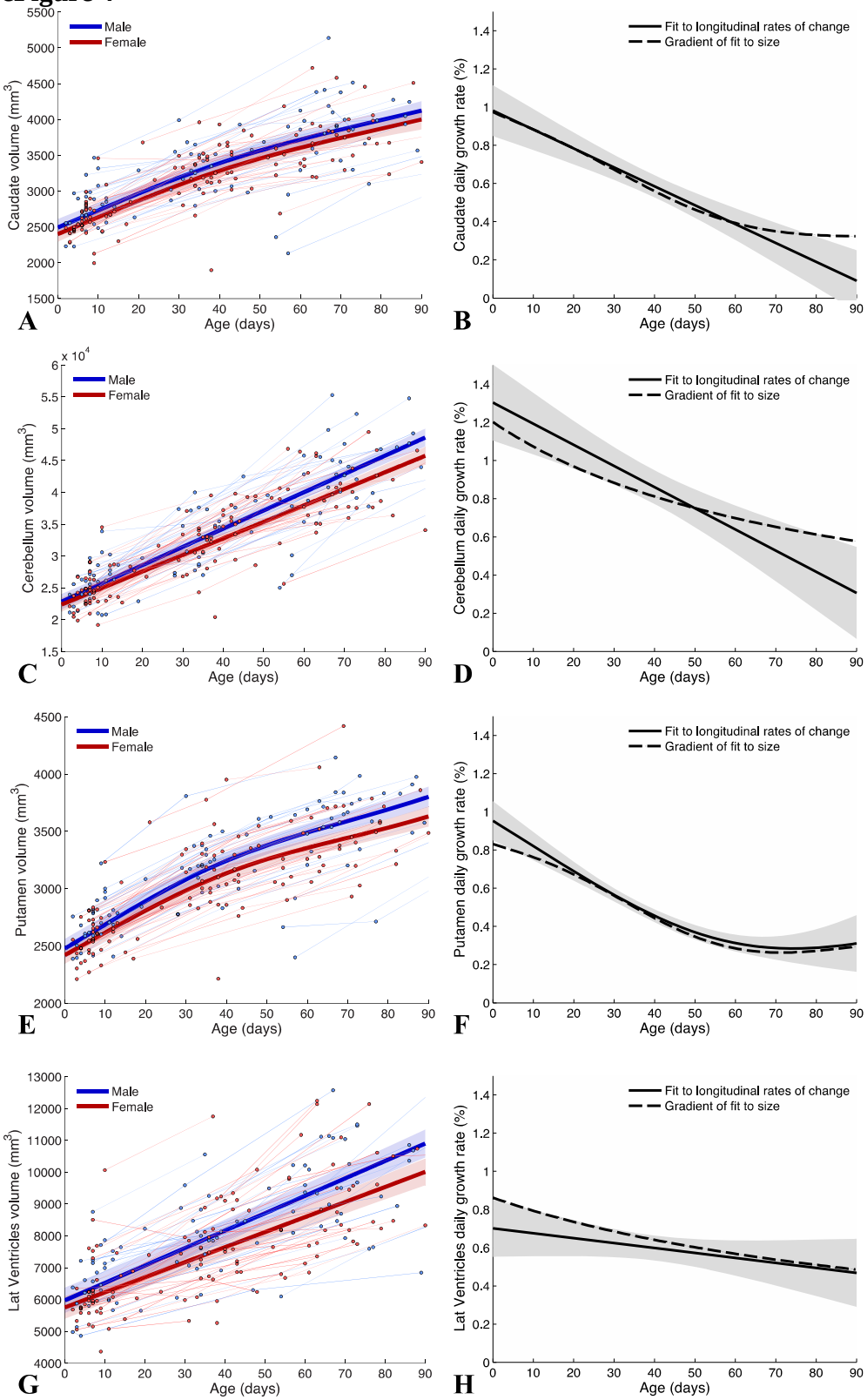

Left column: Spaghetti plots showing volume during the first three months of postnatal life, along with GAMM fits to the data (dark lines, from Eqn. (1)), and 95% confidence intervals (shaded regions). Right column: Daily growth rate during the first three months of postnatal life (for males and females combined). The dashed line is the gradient of a GAMM fit for volume trajectory; the solid line is a GAMM fit to centered linear estimates of the growth rates (between each subject's neighboring data points) from the longitudinal data only. (A-B) caudate, (C-D) cerebellum, (E-F) putamen, (G-H) lateral ventricles.

eFigure 5

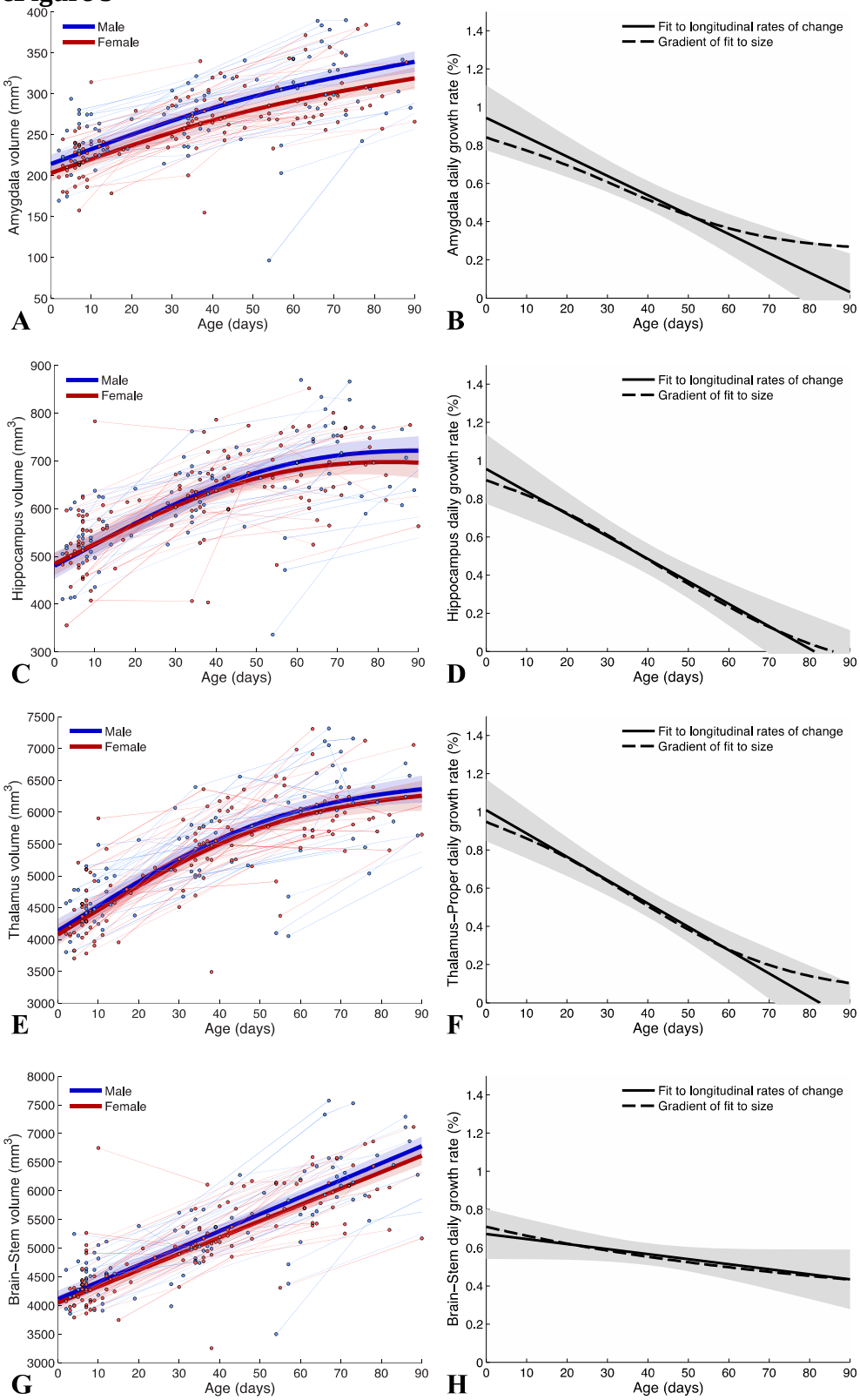

See eFigure 6, but for: (A-B) amygdala, (C-D) hippocampus, (E-F) thalamus, (G-H) brain stem.

eFigure 6.

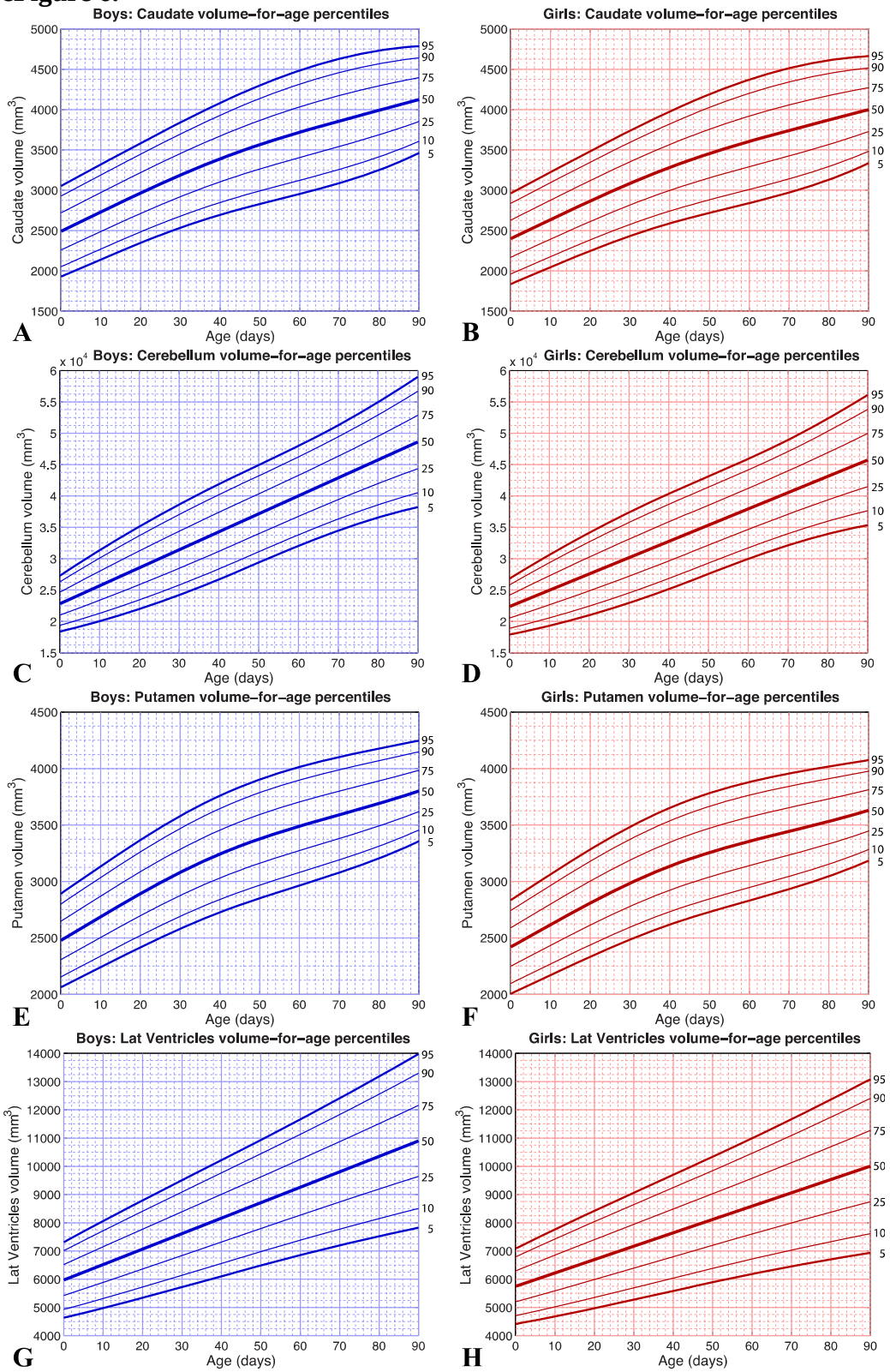

Volume-by age percentile plots for boys (left), and for girls (right): (A-B) caudate; (C-D) cerebellum; (E-F) putamen; (G-H) lateral ventricles.

eFigure 7

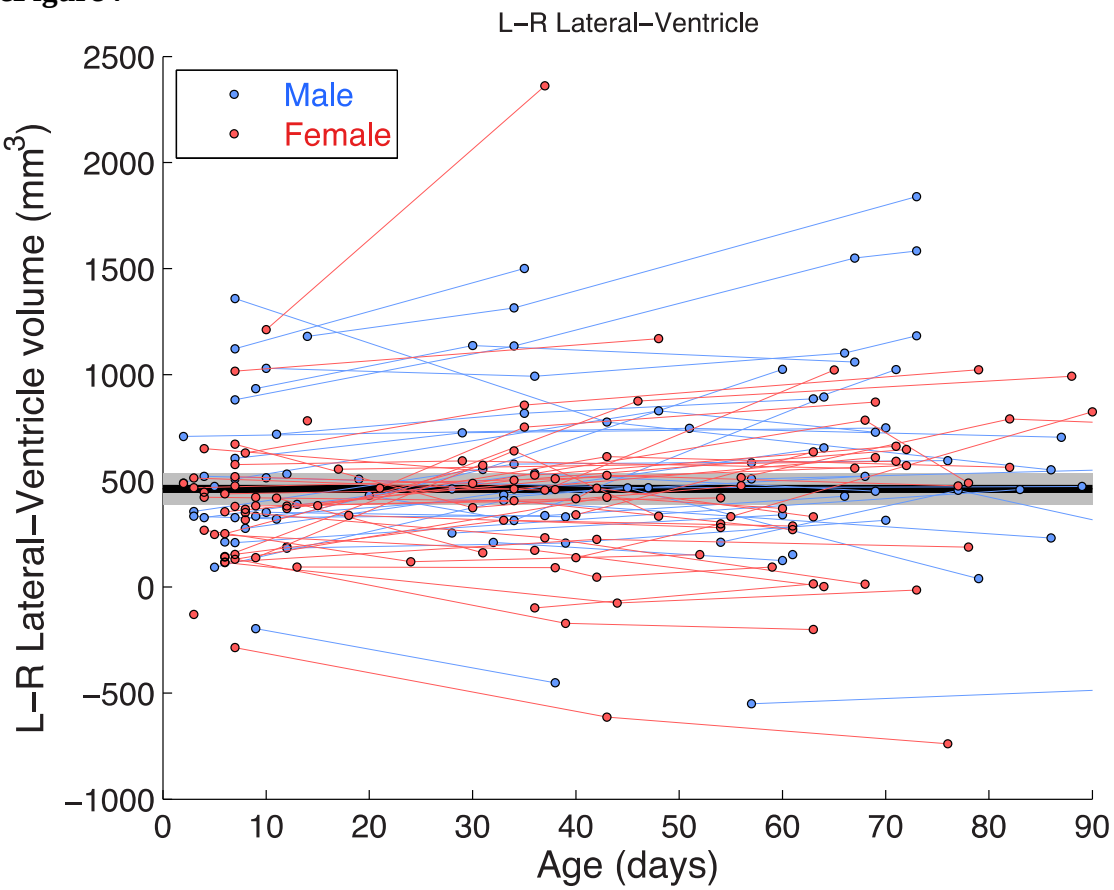

Spaghetti plot of volume difference between left and right lateral ventricles, together with an intercept fit. The black line is a GAMM intercept fit to all the data (regardless of sex), but is overlaid on a sex-specific spaghetti plot of the left-minus-right differences for each subject at each timepoint.

eFigure 8.

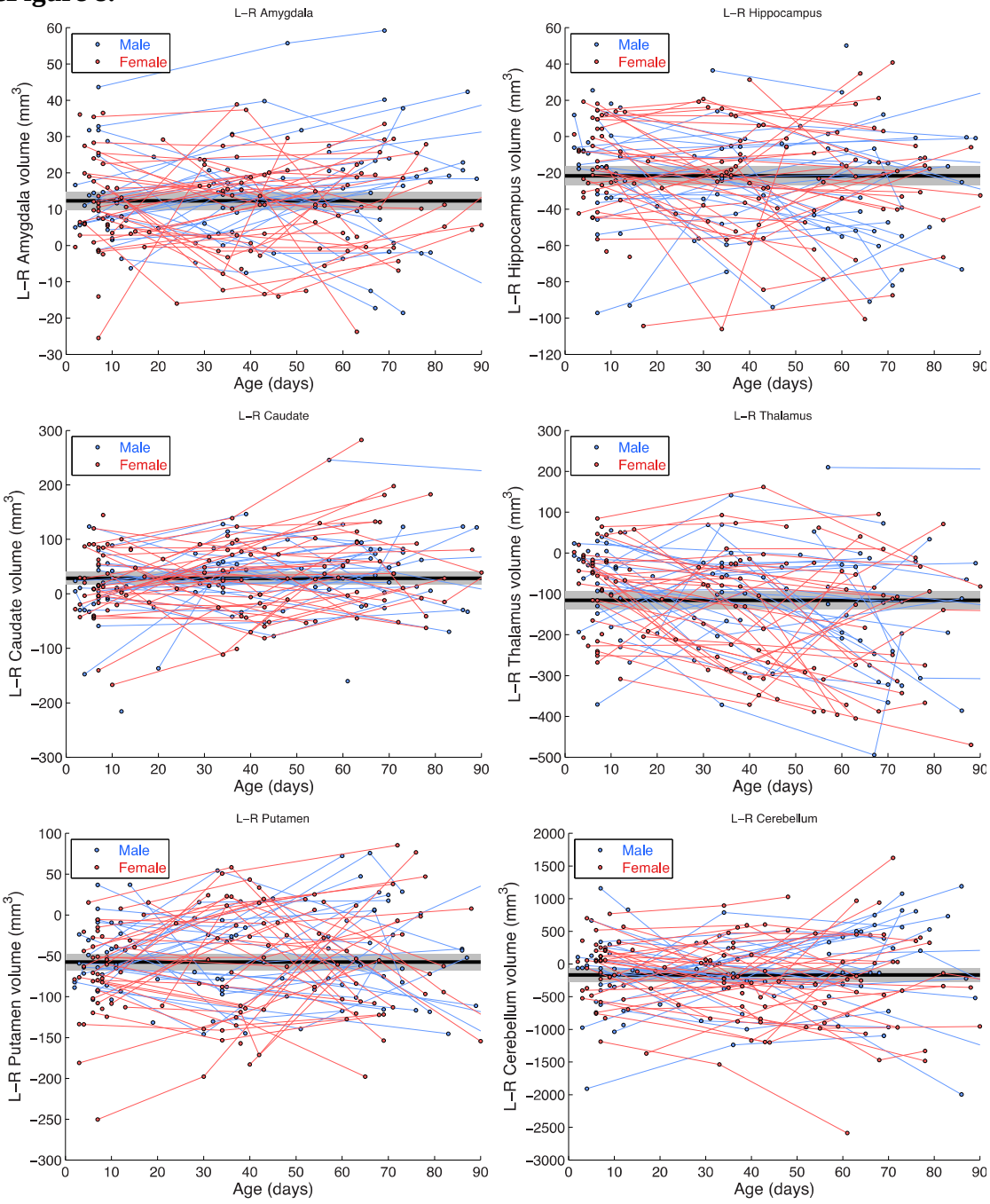

Spaghetti plots of volume difference between left and right ROIs, for amygdala, hippocampus, caudate, thalamus, putamen, and cerebellum. See caption for eFigure 7.

eReferences

1. Roizen NJ, Patterson D. Down's syndrome. *Lancet.* Apr 12 2003;361(9365):1281-1289.
2. Fidler DJ, Hepburn S, Rogers S. Early learning and adaptive behaviour in toddlers with Down syndrome: evidence for an emerging behavioural phenotype? *Downs Syndr Res Pract.* Jun 2006;9(3):37-44.
3. Jernigan TL, Bellugi U, Sowell E, Doherty S, Hesselink JR. Cerebral morphologic distinctions between Williams and Down syndromes. *Arch Neurol.* Feb 1993;50(2):186-191.
4. Kates WR, Folley BS, Lanham DC, Capone GT, Kaufmann WE. Cerebral growth in Fragile X syndrome: review and comparison with Down syndrome. *Microsc Res Tech.* May 1 2002;57(3):159-167.
5. Hessl D, Rivera SM, Reiss AL. The neuroanatomy and neuroendocrinology of fragile X syndrome. *Ment Retard Dev Disabil Res Rev.* 2004;10(1):17-24.
6. Hazlett HC, Poe MD, Gerig G, et al. Early brain overgrowth in autism associated with an increase in cortical surface area before age 2 years. *Arch Gen Psychiatry.* May 2011;68(5):467-476.
7. Nicolson R, Rapoport JL. Childhood-onset schizophrenia: rare but worth studying. *Biol Psychiatry.* Nov 15 1999;46(10):1418-1428.
8. de Vries LS, Groenendaal F. Patterns of neonatal hypoxic-ischaemic brain injury. *Neuroradiology.* Jun 2010;52(6):555-566.
9. Hille ET, Weisglas-Kuperus N, van Goudoever JB, et al. Functional outcomes and participation in young adulthood for very preterm and very low birth weight infants: the Dutch Project on Preterm and Small for Gestational Age Infants at 19 years of age. *Pediatrics.* Sep 2007;120(3):e587-595.
10. Johnson S, Hollis C, Kochhar P, Hennessy E, Wolke D, Marlow N. Psychiatric disorders in extremely preterm children: longitudinal finding at age 11 years in the EPICure study. *J Am Acad Child Adolesc Psychiatry.* May 2010;49(5):453-463 e451.
11. Wintermark P. The role of brain MRI scanning in the newborn. *Paediatrics and Child Health.* April 2012;22(4):155-159.
12. Engle WA. Age terminology during the perinatal period. *Pediatrics.* Nov 2004;114(5):1362-1364.
13. Holland D, Brewer JB, Hagler DJ, Fennema-Notestine C, Dale AM. Subregional neuroanatomical change as a biomarker for Alzheimer's disease. *Proc Natl Acad Sci U S A.* Dec 8 2009;106(49):20954-20959.
14. Holland D, Dale AM. Nonlinear registration of longitudinal images and measurement of change in regions of interest. *Med Image Anal.* Aug 2011;15(4):489-497.
15. Holland D, McEvoy LK, Dale AM. Unbiased comparison of sample size estimates from longitudinal structural measures in ADNI. *Hum Brain Mapp.* Nov 2012;33(11):2586-2602.
16. Kapur T, Grimson WE, Wells WM, 3rd, Kikinis R. Segmentation of brain tissue from magnetic resonance images. *Med Image Anal.* Jun 1996;1(2):109-127.

17. Maes F, Collignon A, Vandermeulen D, Marchal G, Suetens P. Multimodality image registration by maximization of mutual information. *IEEE Trans Med Imaging.* Apr 1997;16(2):187-198.
18. Collins DL, Holmes, C. J., Peters, T. M. and Evans, A. C. Automatic 3-D model-based neuroanatomical segmentation. *Hum. Brain Mapp.* 1995;3(3):190–208.
19. Riddle WR, DonLevy SC, Lee H. Modeling brain tissue volumes over the lifespan: quantitative analysis of postmortem weights and in vivo MR images. *Magn Reson Imaging.* Jun 2010;28(5):716-720.
20. Tamnes CK, Walhovd KB, Dale AM, et al. Brain development and aging: overlapping and unique patterns of change. *Neuroimage.* Mar 2013;68:63-74.
21. Groeschel S, Vollmer B, King MD, Connelly A. Developmental changes in cerebral grey and white matter volume from infancy to adulthood. *Int J Dev Neurosci.* Oct 2010;28(6):481-489.
22. Walhovd KB, Fjell AM, Reinvang I, et al. Effects of age on volumes of cortex, white matter and subcortical structures. *Neurobiol Aging.* Oct 2005;26(9):1261-1270; discussion 1275-1268.